

# PROCEEDINGS OF SPIE

SPIEDigitalLibrary.org/conference-proceedings-of-spie

## Sound speed estimation in layered media using the angular coherence of plane waves

Ali, Rehman, Maredia, Sharil, Telichko, Arsenii, Wang, Huaijun, Paulmurugan, Ramasamy, et al.

Rehman Ali, Sharil Maredia, Arsenii Telichko, Huaijun Wang, Ramasamy Paulmurugan, Jose Vilches-Moure, Jeremy Dahl, "Sound speed estimation in layered media using the angular coherence of plane waves," Proc. SPIE 11319, Medical Imaging 2020: Ultrasonic Imaging and Tomography, 113190F (16 March 2020); doi: 10.1117/12.2548878

**SPIE.**

Event: SPIE Medical Imaging, 2020, Houston, Texas, United States

# Sound Speed Estimation in Layered Media Using the Angular Coherence of Plane Waves

Rehman Ali<sup>a</sup>, Sharil Maredia<sup>b</sup>, Arsenii Telichko<sup>c</sup>, Huaijun Wang<sup>d</sup>, Ramasamy Paulmurugan<sup>e</sup>, Jose Vilches-Moure<sup>f</sup>, and Jeremy Dahl<sup>g</sup>

<sup>a</sup>Department of Electrical Engineering, Stanford University, Palo Alto, CA, 94305 USA

<sup>b</sup>Clear Springs High School, League City, TX, 77573 USA

<sup>c,d,e,g</sup>Department of Radiology, Stanford School of Medicine, Palo Alto, CA, 94304 USA

<sup>f</sup>Comparative Medicine, Stanford University Medical Center, Palo Alto, CA, 94304 USA

## ABSTRACT

We present a refraction-corrected sound speed reconstruction technique for layered media based on the angular coherence of plane waves. Previous work has successfully shown that sound speed estimation and refraction-corrected image reconstruction can be achieved using the coherence of full-synthetic aperture channel data. However, methods for acquiring the full-synthetic aperture dataset require a large number of transmissions, which can confound sound speed estimation due to the scatterer motion between transmit events, especially for in-vivo application. Furthermore, sound speed estimation requires producing full-synthetic aperture coherence images for each trial sound speed, which can make the overall computational cost quite burdensome. The angular coherence beamformer, initially devised as a quicker alternative to the more conventional spatial coherence beamformer, measures coherence between fully-beamformed I/Q channel data for each plane wave as opposed to the receive channel data prior to receive beamforming. As a result, angular coherence beamforming can significantly reduce the computation time needed to reconstruct a coherence image by taking advantage of receive beamforming. Previous work has used the coherence maximization of full-synthetic aperture channel data to perform sound speed estimation. By replacing spatial coherence with angular coherence, we apply a similar methodology to channel data from plane-waves to significantly reduce the computational cost of sound speed estimation. This methodology has been confirmed by both simulated and experimental channel data from plane waves.

**Keywords:** Plane-Wave Imaging, Angular Coherence, Sound Speed Estimation, Layered Media

## 1. INTRODUCTION

The goal of sound speed estimation in medical ultrasound is to measure the sound speed of human tissue in an accurate and spatially-resolved manner. One application of sound speed estimation is fat quantification in human liver for fatty liver disease.<sup>1</sup> A reasonable model of the liver and superficial abdominal layers assumes that sound speed in the medium varies primarily as a function of depth. In this model, the effective average sound speed up to a particular depth can be related to the local sound speed as a function of depth.<sup>2,3</sup> The effective average sound speed up to each depth is measured using coherence maximization. Model inversion allows reconstruction of the local sound speed at each depth from the average sound speed measurements.

One of the methods previously employed to perform sound speed estimation in layered media is based on image-registration.<sup>4</sup> This approach models each imaging line as a ray whose refracted path is modeled using Snell's law. Refraction is used to model the geometric transformations applied to beamformed ultrasound images at each steering angle. The sound speed in the medium is determined by maximizing the alignment of the ultrasound images produced at each transmission angle as a result of applying these geometric transformations. Borrowing from this approach, our methodology adjusts both receiver delays and the assumed transmission angle as a function of sound speed in the medium. A stack of angled plane-wave I/Q images are formed at each candidate sound speed. The effective average sound speed is determined by maximizing the coherence across

---

Further author information: (Send correspondence to Rehman Ali)  
Rehman Ali: E-mail: rali8@stanford.edu

angles in this stack of plane-wave I/Q images at each depth. Note that angular coherence<sup>5</sup> reduces acquisition and computation time over spatial coherence<sup>6</sup> by acquiring channel data from plane waves, which often require much fewer transmit events, and by taking advantage of dynamic-receive focusing.

By adjusting both receiver delays and transmission angles as a function of sound speed, plane-wave imaging can be used to accurately estimate sound speed in a layered medium. Recent works<sup>7,8</sup> have also considered sound speed estimation in media where significant lateral sound speed variations are present. Because these approaches are based on phase aberrations measured between plane-wave images at different angles rather than absolute travel times, they result in sound speed estimates that have high lateral resolution but poor axial resolution. The goal of this work is to show that the same imaging setup can be used to achieve high axial resolution and accuracy.

## 2. BACKGROUND

### 2.1 Coherence Imaging with Plane Wave Transmissions

Beamforming channel data from plane-wave transmits requires knowledge of both transmit and receive travel times to and from a scattering location  $(x, z)$ . The start time ( $t = 0$ ) for each plane wave is considered to be the time that the center of the transmit pulse emits from  $(0, 0)$  on the transducer array. The time it takes for a plane wave at angle  $\theta$  to reach  $(x, z)$  from  $(0, 0)$  in a medium with sound speed  $c$  is

$$\tau_{tx}(x, z; \theta, c) = \frac{x \sin \theta + z \cos \theta}{c}. \quad (1)$$

Note that plane waves are transmitted at angles  $\theta_{assumed}$  with an assumed sound speed of  $c_{assumed}$  in the medium. If the true sound speed in the medium is  $c$ , then the true transmission angle  $\theta$  by Snell's law is

$$\theta(c; \theta_{assumed}, c_{assumed}) = \arcsin\left(\frac{c \sin \theta_{assumed}}{c_{assumed}}\right). \quad (2)$$

The time it takes for sound scattered at  $(x, z)$  to arrive at a receiver located at  $(x_{rx}, 0)$  is

$$\tau_{rx}(x, z; \theta, c) = \frac{\sqrt{(x - x_{rx})^2 + z^2}}{c}. \quad (3)$$

Given I/Q receive channel data  $s(t; \theta_{assumed}, x_{rx})$  as a function of  $\theta_{assumed}$ ,  $x_{rx}$ , and time  $t$ , each angled plane-wave image  $I(x, z; \theta_{assumed}, c)$  can be computed as

$$I(x, z; \theta_{assumed}, c) = \sum_{x_{rx}} s(\tau_{tx}(x, z; \theta(c; \theta_{assumed}, c_{assumed}), c) + \tau_{rx}(x, z; x_{rx}, c); \theta_{assumed}, x_{rx}), \quad (4)$$

where the sum is computed over all receivers. A naive approach would be to neglect that the true angle of transmission varies with the speed of sound in the medium and assume a fixed set of transmit angles  $\theta_{assumed}$ . The plane-wave image based on this naive approach would be written as

$$I(x, z; \theta_{assumed}, c) = \sum_{x_{rx}} s(\tau_{tx}(x, z; \theta_{assumed}, c) + \tau_{rx}(x, z; x_{rx}, c); \theta_{assumed}, x_{rx}). \quad (5)$$

Accurate modeling of the change in transmission angle as function of sound speed is important for the sound speed estimation process. Results show a comparison of the naive approach in equation (5) to the angle-corrected approach in equation (4) in our sound speed estimation process. An angular coherence factor (CF) image<sup>5,9</sup> is produced by computing a coherent sum over an incoherent sum across  $N$  angled plane-wave images:

$$CF(x, z; c) = \frac{|\sum_{\theta_{assumed}} I(x, z; \theta_{assumed}, c)|^2}{N \sum_{\theta_{assumed}} |I(x, z; \theta_{assumed}, c)|^2}. \quad (6)$$

## 2.2 Layered Medium Model

In a layered medium that permits sound speed variation in the  $z$ -direction but not the  $x$ -direction, the effective average sound speed  $c_{avg}(z)$  up to depth  $z$  is related to the local sound speed  $c_{local}(z)$  at depth  $z$  by the integral

$$\frac{1}{c_{avg}(z)} = \frac{1}{z} \int_0^z \frac{dz}{c_{local}(z)}. \quad (7)$$

The effective average sound speed  $c_{avg}(z)$  can be measured by coherence maximization:

$$c_{avg}(z) = \arg \min_c \left( \sum_x CF(x, z; c) \right), \quad (8)$$

The local sound speed  $c_{local}(z)$  at each depth  $z$  can be computed by inverting (7) to get

$$\frac{1}{c_{local}(z)} = \frac{d}{dz} \left( \frac{z}{c_{avg}(z)} \right). \quad (9)$$

## 3. METHODS

### 3.1 Simulation of Channel Data from Plane Waves

Field II and k-Wave were used to simulate full-synthetic aperture channel data from media with diffuse scatterers using a 128-element transducer array with 0.15 mm pitch. Field II was used to simulate media with constant sound speed. The sound speeds in the media simulated by Field II ranged from 1480 to 1600 m/s in steps of 10 m/s. Furthermore, Gaussian pulses with 70% fractional bandwidth and center frequencies ranging from 2 to 10 MHz (in 1 MHz steps) were simulated for each media. K-Wave was used to simulate layered media where sound speed varied as a function of depth. First, a series of two-layered media is simulated where the first 15 mm of the media has 1480 m/s sound speed and the remainder of the media has either 1520, 1540, or 1570 m/s sound speed. Twelve different scatterer realizations were simulated for each of the three two-layered media in order to measure statistical variations in local sound speed estimates. Each of these k-Wave simulations were repeated for 4 and 8 MHz Gaussian transmit pulses with 70% fractional bandwidth. Finally, k-Wave was also used to simulate media with 4, 5, and 8 layers whose sound speeds were randomly assigned from 1480 m/s to 1600 m/s. Each of these k-Wave simulations used an 8 MHz, 70% fractional bandwidth, Gaussian transmit pulse. Channel data for plane waves were synthesized from the full-synthetic aperture dataset. Each plane wave dataset consists of 5 equally-spaced plane waves ranging from  $\theta_{assumed} = -\frac{\pi}{12}$  to  $\theta_{assumed} = \frac{\pi}{12}$  at  $c_{assumed} = 1540 \frac{m}{s}$ .

### 3.2 Experimental Datasets

The Verasonics Vantage 256 scanner was used to acquire plane-wave channel data from an ATS Model 549 speckle phantom and chicken breast using an L11-5 ultrasound probe. The plane-wave transmit sequence used in these experiments consisted of 33 plane waves ranging from -20 to 20 degrees in angle. The Verasonics Vantage 256 scanner was also used to acquire full-synthetic aperture channel data from obese Zucker rats using an L12-3v probe. A dataset consisting of plane-waves ranging from -30 to 30 degrees was constructed from each full-synthetic aperture dataset. These experiments were used to estimate the speed of sound in the liver through the abdominal wall. The resulting sound speed estimates in each rat were compared to direct measurements<sup>10,11</sup> made on the excised liver using a piston transducer, pulser-receiver, and oscilloscope.

## 4. RESULTS AND DISCUSSION

Our goal is to first validate the sound speed estimation methodology in homogeneous media. A key aspect of our sound speed estimator is correcting the angle of the plane wave based on the sound speed in the medium (equation (2)). The naive approach to sound speed estimation with plane waves applies coherence maximization over a set of fixed transmission angles that do not vary as function of sound speed. Figure 1 shows that when the true speed of sound in the medium is far from  $c_{assumed}$ , the peak coherence decreases in the naive approach (equation (5)) compared to the angle-corrected approach (4)). Furthermore, in the absence of Snell's law correction, the

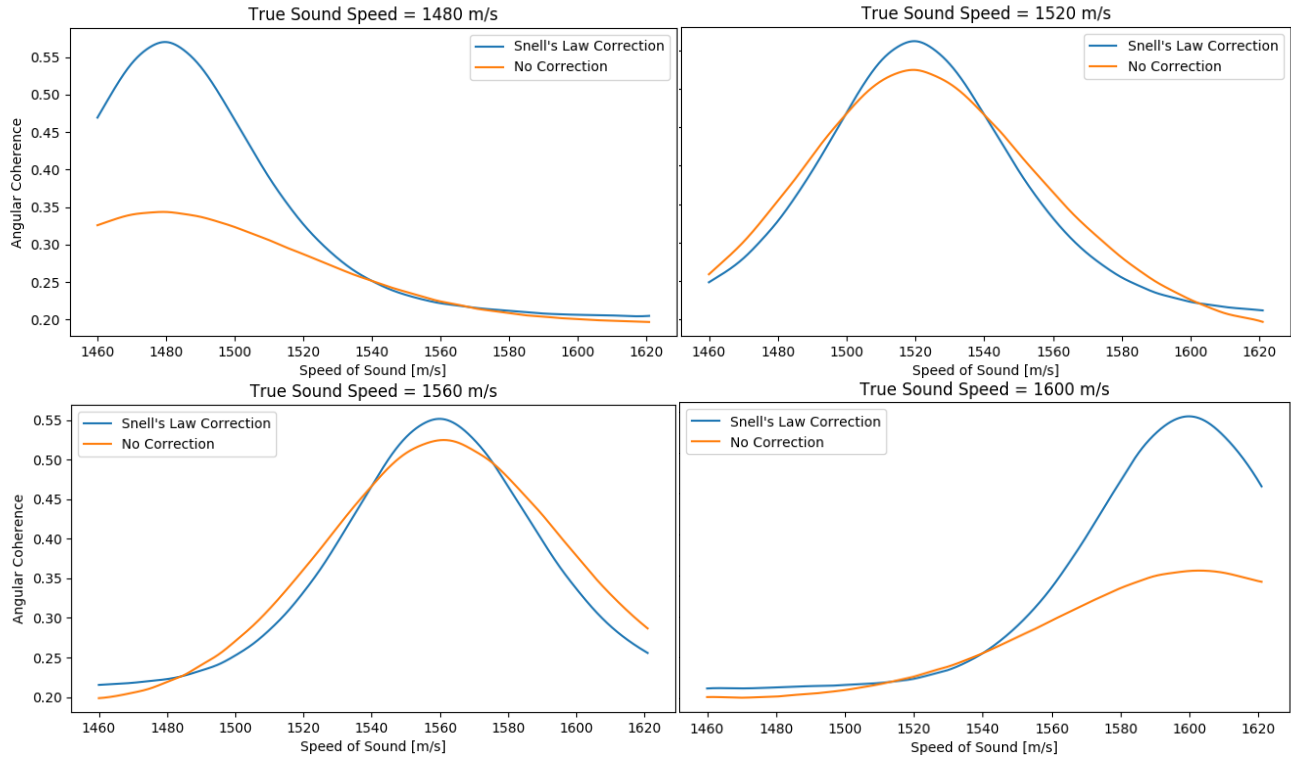


Figure 1. Importance of Snell's law correction to sound speed estimation based on plane-waves. The angular CF was averaged within an ROI ranging from 15 to 25 mm in depth and -5 to 5 mm laterally. Sound speed estimation was performed at 8 MHz center frequency in media with 1480 (upper left), 1520 (upper right), 1560 (lower left) and 1600 m/s (lower right) sound speeds. The maximum angular CF is much lower without Snell's law correction. The estimated sound speeds with a Snell's law correction are 1479.7, 1519.7, 1559.9, and 1599.8 m/s, for each plot respectively. Without a correction, the estimated sound speeds are 1479.1, 1519.4, 1561.1, and 1602.8 m/s, respectively. The difference between angular CF curves with and without Snell's law correction is minimal for the media at 1520 and 1560 m/s sound speed, mainly because the speed of sound in these media is close to the  $c_{\text{assumed}}$  of 1540 m/s

speed of sound at which the peak coherence is achieved tends to be further from the true speed of sound in the medium.

Figure 2 demonstrates how the angular CF focusing metric changes as a function of frequency. Since sound speed error results in phase variation across the aperture, an increase in the imaging frequency should further accelerate phase variation across the aperture. Thus, as the frequency increases, the angular CF becomes narrower around the true speed of sound in the medium, decreasing the uncertainty of our sound speed estimate.

Figure 3 shows that for plane-wave sequences with a fixed angular extent, the angular CF has similar behavior near the peak. However, angular CF finds an asymptotic plateau as the beamforming speed of sound goes away from the true speed of sound in the medium. The height of this plateau decreases as the number of plane-wave angles decreases for a fixed angular span. This plateau effect can be understood as the result of insufficient angular sampling. As the beamforming speed of sound gets further from the true speed of sound in the medium, the phase shifts between each angled plane-wave image become aliased. This aliasing results in a roughly constant angular CF for large sound speed errors.

Figure 4 shows that angular CF becomes tighter around the true speed of sound as the angular extent of the plane-wave sequence increases. It is expected that angular CF decreases overall and becomes narrower as the angular extent increases because the increase in angular extent captures more phase variation for the same set of imaging points.

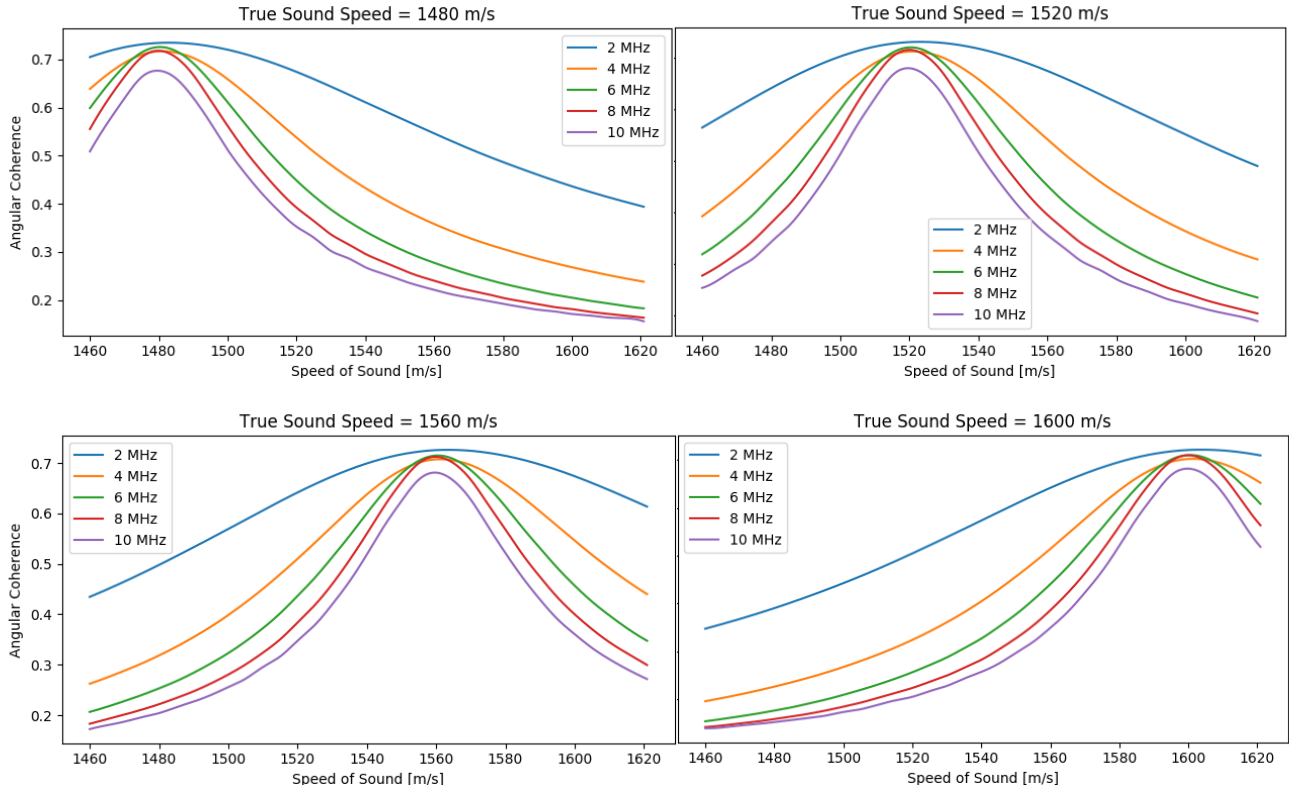


Figure 2. Sound speed estimation by angular CF maximization at different frequencies. The frequency dependence of coherence factor maximization is examined in media with four different speeds of sound: 1480 (upper left), 1520 (upper right), 1560 (lower left), and 1600 m/s (lower right). Angular CF reaches its maximum when the reconstruction sound speed is close to the true sound speed in the medium. As the pulse frequency increases, the curve of angular CF vs reconstruction sound speed becomes tighter.

Figure 5 shows that angular CF decreases and widens around the true speed of sound in the medium as the imaging depth increases. However, as sound speed errors increase, the curves of angular CF behaves similarly at the tails. However, the change in angular CF as a function of depth has a negligible effect on sound speed estimation.

All the results shown thus far characterize (global) average sound speed estimation in homogeneous media. These results should translate to our ability to measure the effective average speed of sound  $c_{avg}(z)$  in layered media. Figure 6 demonstrates the complete sound speed estimation procedure for a two-layer medium using equation (9). The top panel shows a color-map of the angular CF as function of depth and average sound speed. The average speed of sound  $c_{avg}(z)$  is taken to be the peak of the angular CF at each depth  $z$ . The resulting average speed of sound was smoothed prior to applying equation (9) to obtain the local sound speed estimates shown in the bottom panel. The mean and standard deviation in local sound speed estimates are shown across 12 different realizations. As the frequency increases, the uncertainty in both the average and local sound speed estimates decreases. The conclusion of these results are similar to the results shown in Figure 2. The complete sound speed estimation methodology is also shown in Figure 7 for layered media with a variety of different sound speeds and number of layers.

Because the sound speed in the speckle phantom (1450 m/s) is far from the  $c_{assumed}$ , the curve of angular CF is much broader and flatter near the peak in the absence of the Snell's law correction (Figure 8). This shape indicates the uncertainty and inaccuracy of the sound speed measurement. We do not find this issue with the chicken breast (meat) because its speed of sound is much closer to the  $c_{assumed}$ . Figure 8 revisits the effect of the number of plane-wave angles for a fixed angular span. In addition to the plateau effect seen in Figure 1, the

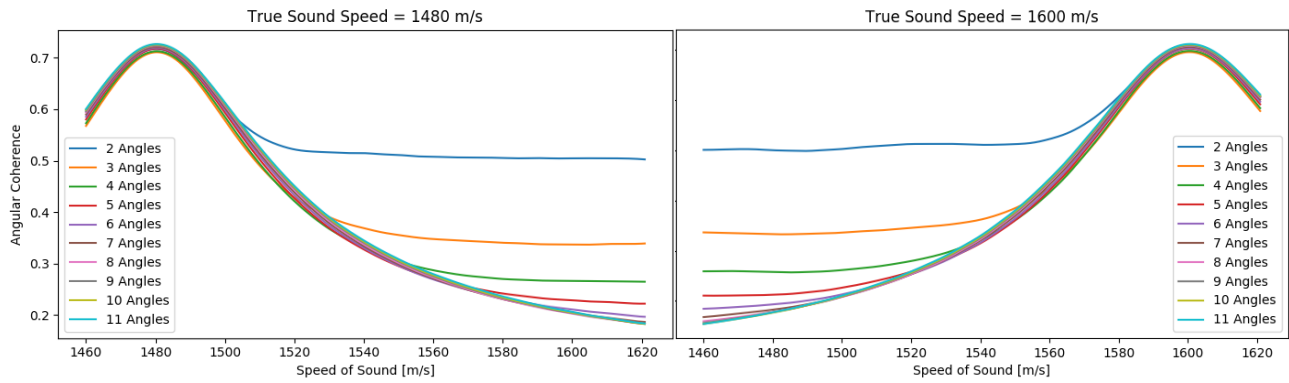


Figure 3. Effect of the number of transmit angles on sound speed estimation by angular CF maximization. Angular CF is plotted against beam-forming speed of sound for media with a true sound speed of 1480 (left) and 1600 m/s (right). In both plots, an increase in the number of angles decreases the angular CF value at the plateau away from the peak of the curve.

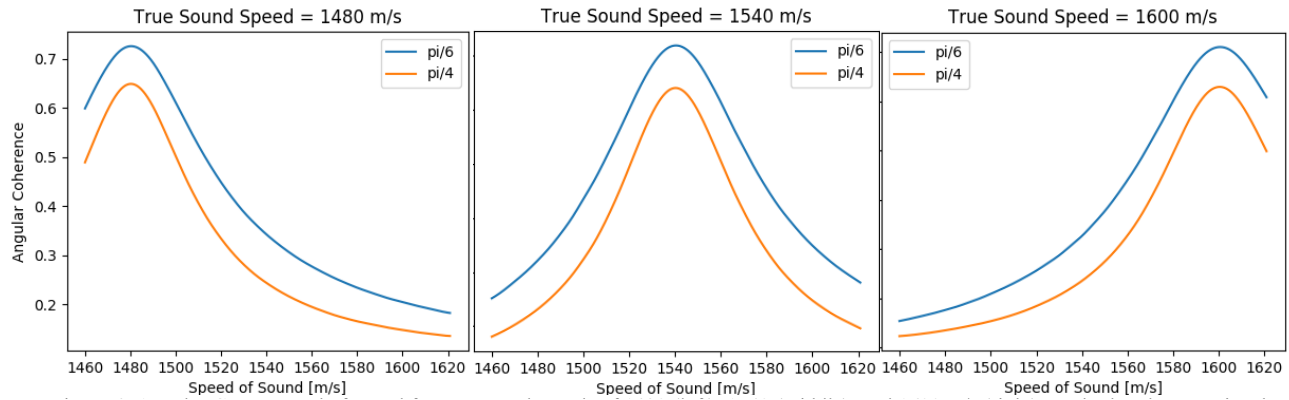


Figure 4. Effect of angular extent on CF maximization in media with 1480 (left), 1540 (middle), and 1600 (right) m/s sound speed. While a total angle of  $\pi/6$  radians has a higher maximum angular CF, a total angle of  $\pi/4$  radians has a narrower curve (FWHM = 84.646 m/s for  $\pi/4$  radians; FWHM = 111.306 m/s for  $\pi/6$  radians).

finite signal-to-noise ratio (SNR) of the experimentally-acquired channel data also appears to have an effect on angular CF as a focusing metric, i.e., the peak of the angular CF curve appears to be proportional to the number of plane-wave angles. The complete sound speed estimation methodology was tested in two obese Zucker rats (Figure 10). In each case, we only consider the sound speed measurements over the first 15 mm into the medium because these are the depths over which lateral variations in the speed of sound are minimal. While the average speed of sound in the liver was far from direct measurement over the excised liver samples, the local speed of sound remained close to the direct measurement in each rat.

## 5. CONCLUSIONS

We extend previous work<sup>2</sup> on coherence-based local sound speed estimation by showing that a similar methodology applies to channel data from plane waves rather than the full-synthetic aperture. Our methodology takes into account both the refraction of the plane wave (as in Krucker et al.<sup>4</sup>) and changes in receiver delays as a function of sound speed in the medium. By adjusting the sound speed used to form the plane wave images, the average sound speed in the medium can be measured by maximizing the coherence across plane waves. The local sound speed in the medium can then be determined from the average sound speed. This plane wave imaging approach can significantly reduce acquisition times and the computational cost of local sound speed estimation. Future work should combine our methodology with tomographic plane-wave-based approaches<sup>7,8</sup> to optimally estimate the local sound speed in an axially- and laterally-varying sound speed medium.

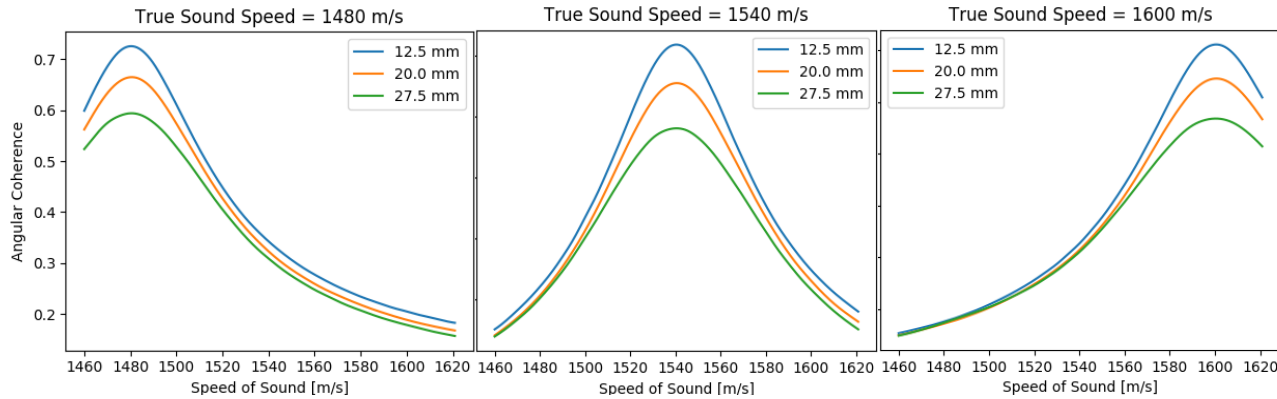


Figure 5. Effect of imaging depth on angular CF as a function of beamforming sound speed in media with 1480 (left), 1540 (middle), and 1600 (right) m/s speed of sound. The angular CF was averaged within an ROI ranging -5 to 5 mm laterally and 10 mm axially centered around 12.5 mm, 20.0 mm, and 27.5 mm in depth. The maximum angular CF decreases with increasing imaging depth. Each CF curve becomes broader with imaging depth (FWHM = 91.52, 93.88, and 99.63 m/s). The sound speed estimates are 1480.3, 1540.4, and 1600.6 m/s at 12.5 mm depth, 1480.6, 1540.6, and 1600.6 m/s at 20.0 mm depth, and 1480.5, 1540.5, and 1600.3 m/s at 27.5 mm depth.

## ACKNOWLEDGMENTS

We would like to acknowledge Joseph Jennings and Dr. Biondo Biondi from the Department of Geophysics at Stanford University for their expertise and advice on velocity estimation in layered media. Finally, we would like to acknowledge the National Defense Science and Engineering Graduate (NDSEG) Fellowship for sponsoring Rehman Ali's graduate research work.

## REFERENCES

- [1] Imbault, M., Faccinetto, A., Osmanski, B.-F., Tissier, A., Deffieux, T., Gennisson, J.-L., Vilgrain, V., and Tanter, M., "Robust sound speed estimation for ultrasound-based hepatic steatosis assessment," *Physics in Medicine & Biology* **62**(9), 3582 (2017).
- [2] Ali, R. and Dahl, J. J., "Distributed phase aberration correction techniques based on local sound speed estimates," in [2018 IEEE International Ultrasonics Symposium (IUS)], 1–4, IEEE (2018).
- [3] Jakovljevic, M., Hsieh, S., Ali, R., Chau Loo Kung, G., Hyun, D., and Dahl, J. J., "Local speed of sound estimation in tissue using pulse-echo ultrasound: Model-based approach," *The Journal of the Acoustical Society of America* **144**(1), 254–266 (2018).
- [4] Krucker, J., Fowlkes, J. B., and Carson, P. L., "Sound speed estimation using automatic ultrasound image registration," *IEEE transactions on ultrasonics, ferroelectrics, and frequency control* **51**(9), 1095–1106 (2004).
- [5] Li, Y. L. and Dahl, J. J., "Angular coherence in ultrasound imaging: Theory and applications," *The Journal of the Acoustical Society of America* **141**(3), 1582–1594 (2017).
- [6] Hyun, D., Crowley, A. L. C., and Dahl, J. J., "Efficient strategies for estimating the spatial coherence of backscatter," *IEEE transactions on ultrasonics, ferroelectrics, and frequency control* **64**(3), 500–513 (2016).
- [7] Jaeger, M., Held, G., Peeters, S., Preisser, S., Grünig, M., and Frenz, M., "Computed ultrasound tomography in echo mode for imaging speed of sound using pulse-echo sonography: proof of principle," *Ultrasound in medicine & biology* **41**(1), 235–250 (2015).
- [8] Sanabria, S. J., Ozkan, E., Rominger, M., and Goksel, O., "Spatial domain reconstruction for imaging speed-of-sound with pulse-echo ultrasound: simulation and in vivo study," *Physics in Medicine & Biology* **63**(21), 215015 (2018).
- [9] Du, B., Wu, X., Zheng, H., Fang, S., Lu, M., and Mao, R., "Coherence plane-wave compounding with angle coherence factor for ultrafast ultrasound imaging," in [2018 40th Annual International Conference of the IEEE Engineering in Medicine and Biology Society (EMBC)], 907–910, IEEE (2018).

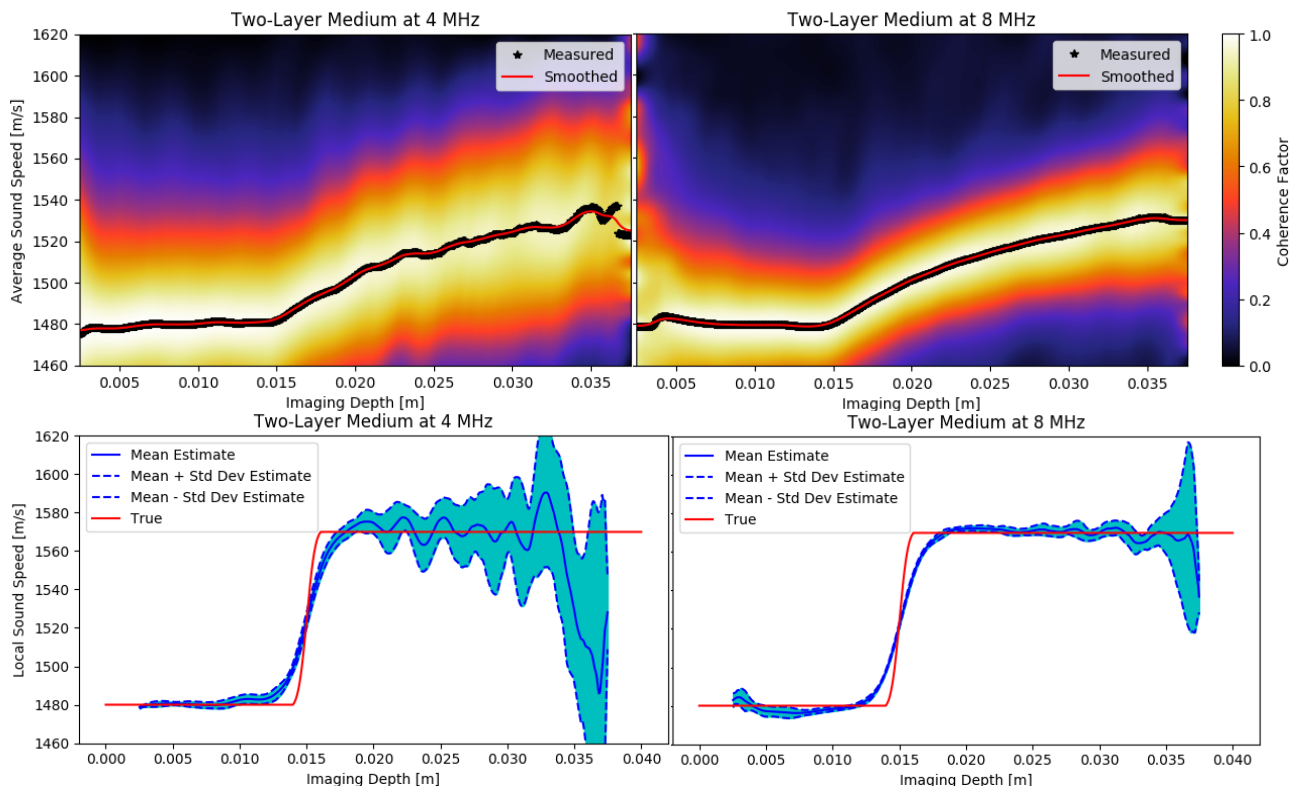


Figure 6. Local sound speed estimation in two-layer media with 1480 m/s in top layer and 1570 m/s in bottom layer using 4 MHz (left) and 8 MHz (right) pulses. The top two plots display the intermediate step for local sound speed estimation, in which the average sound speed with the highest angular CF is calculated for each imaging depth. The bottom two plots show the reported mean and standard deviation of local sound speed estimates measured across 12 different speckle realizations. The standard deviation in local sound speed estimates decreases when going from 4 to 8 MHz transmit frequency.

- [10] Kuo, I., Hete, B., and Shung, K., “A novel method for the measurement of acoustic speed,” *The Journal of the Acoustical Society of America* **88**(4), 1679–1682 (1990).
- [11] Hachiya, H., Ohtsuki, S., Tanaka, M., and Dunn, F., “Determination of sound speed in biological tissues based on frequency analysis of pulse response,” *The Journal of the Acoustical Society of America* **92**(3), 1564–1568 (1992).

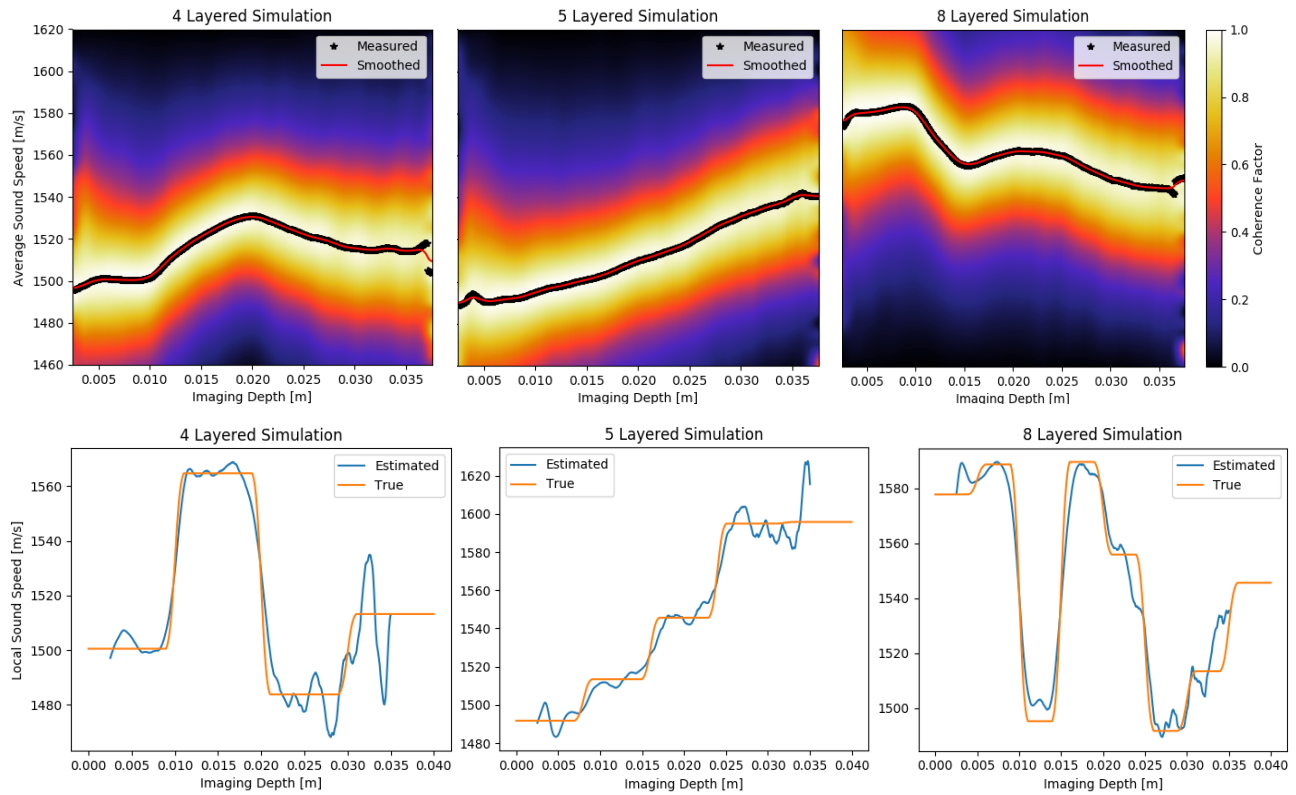


Figure 7. Local sound speed estimation in media with multiple layers with varying speeds of sound in each layer. The top three plots demonstrate the intermediate step in which the average sound speed with the highest angular CF is calculated for each imaging depth. The bottom three plots demonstrate that this sound speed estimation process can be performed in media with more than two layers.

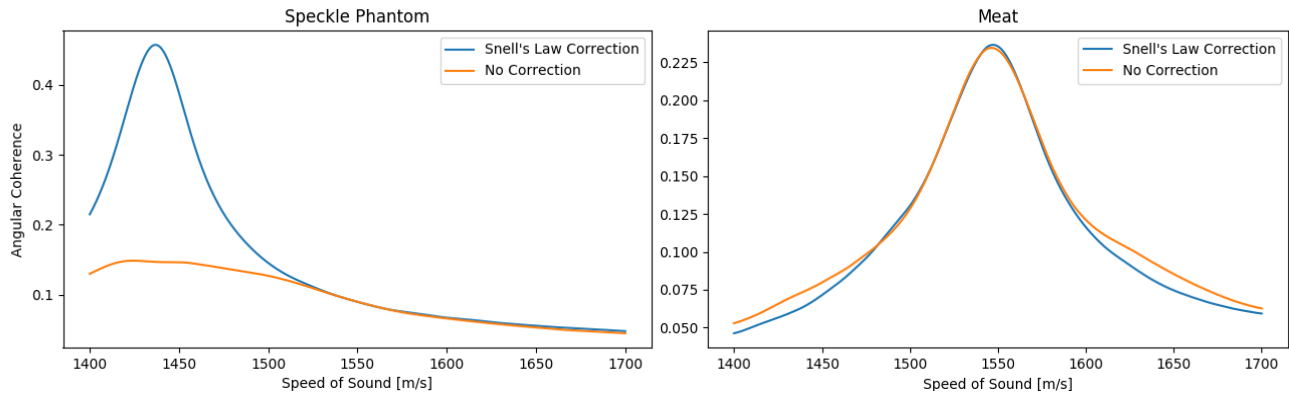


Figure 8. Experimental demonstration of the necessity of Snell's law correction in sound speed estimation based on plane waves. Plane-wave channel data from an ATS 549 speckle phantom (left) and chicken breast meat (right) were gathered from an L11-5 transducer on the Verasonics Vantage 256 system. For the speckle phantom (true sound speed of 1450 m/s, subject to temperature variations), the estimated sound speed was 1436.8 m/s with an angle correction, but 1424.2 m/s without an angle correction. Furthermore, the peak in angular CF was much lower for the meat (typically 1550–1560 m/s), the estimated sound speed was 1547.2 m/s with an angle correction, but 1546.3 m/s without an angle correction. In both cases, the speed of sound appears to be lower than typical values due to the recent refrigeration of the meat and contact with the phantom. Sound speed typically decreases as temperature decreases.

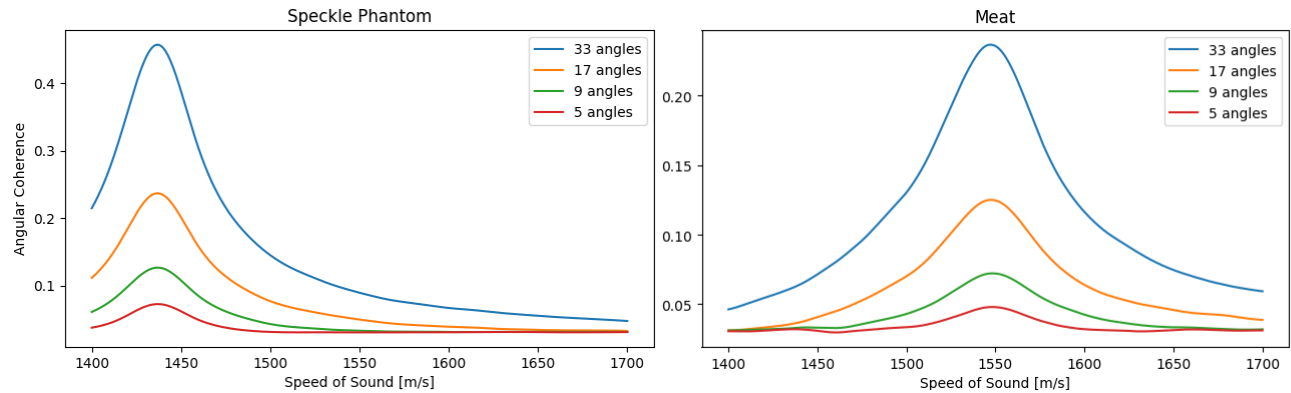


Figure 9. Experimental demonstration of the effect of the number of transmit angles on sound speed estimation by angular CF maximization. For each of the ATS 549 speckle phantom (left), and chicken meat (right), as the number of angles decreases, the peak angular CF decreases as the total number of plane-wave transmits decreases for a fixed total angle of 40 degrees. This trend in the peak angular CF, which is not observed in the simulated datasets shown in Figure 3, is mainly due to the finite signal-to-noise ratio (SNR) of the experimental data acquisition.

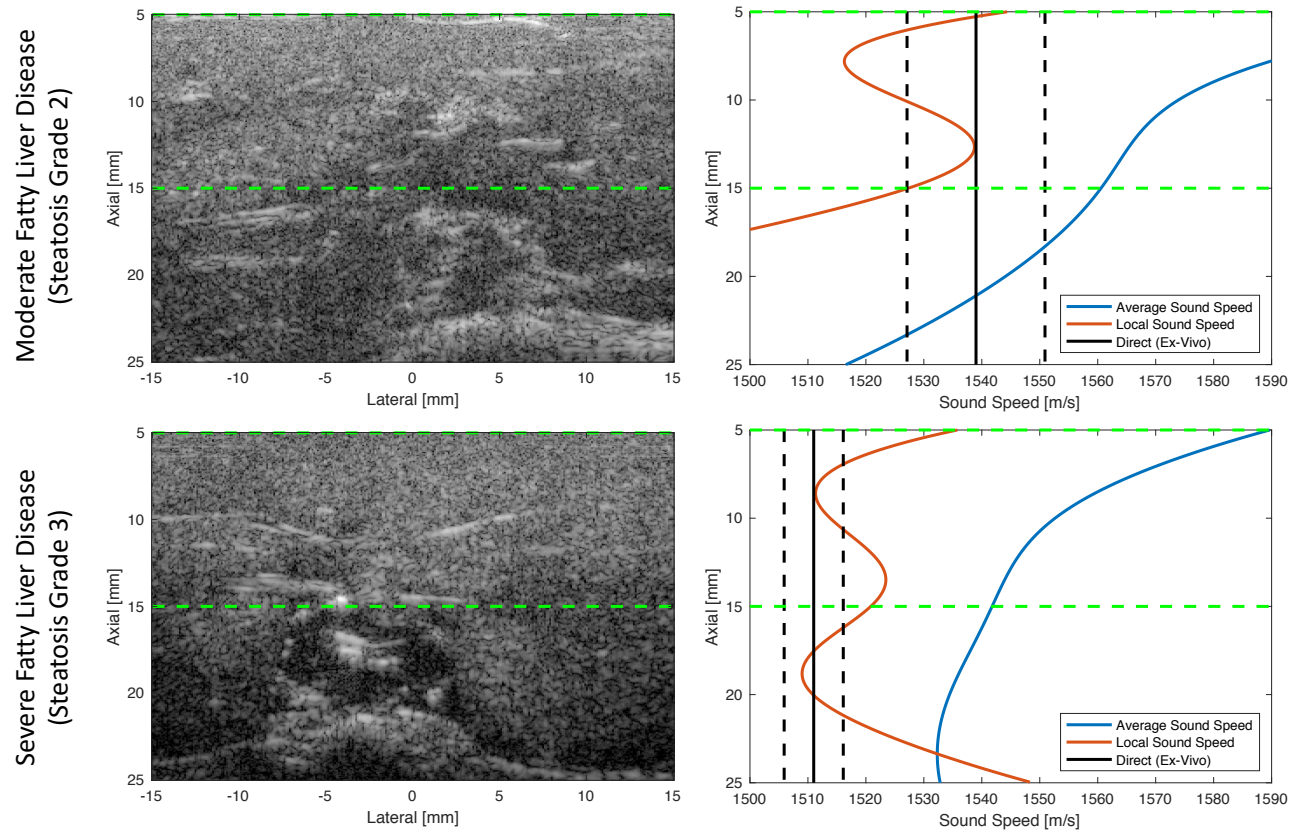


Figure 10. Average and local sound speed estimates in obese Zucker rats. In rats with both moderate (top) and severe (bottom) fatty liver disease, local sound speed estimates appear to agree well with ex-vivo sound speed measurements (mean and standard deviation are indicated by solid and dashed black lines). In each case, the average sound speed estimate is far from the speed of sound in the liver due to the high speed of sound in the overlying abdominal layers.